Mechanical Characterization of Low Modulus Polymer-Modified Calcium-Silicate-Hydrate (C-S-H) Binder

Starr, J.[a], Soliman, E. M.[b], Matteo, E. N.[c], Dewers, T.[c], Stormont, J.[a] Reda Taha, M. M.[a,*]

[a] Department of Civil, Construction & Environmental Engineering, University of New Mexico, MSC01 1070, 1 University of New Mexico, NM 87131, USA
[b] Civil Engineering Department, Faculty of Engineering, Assiut University, Assiut, Egypt, 71516.
[c] Sandia National Laboratories, Albuquerque, NM, 87131, Zip Code USA

[*]Author to whom all correspondence to be addressed. Department of Civil, Construction & Environmental Engineering, MSC01 1070, 1 University of New Mexico, Albuquerque, NM 87131-0001, E-mail: mrtaha@unm.edu Phone: 505- 277-1258, Fax: 505-277-1988

ABSTRACT

Calcium-silicate-hydrate (C-S-H) represents a key microstructural phase that governs the mechanical properties of concrete at a large scale. Defects in the C-S-H phase are also responsible for the poor ductility and low tensile strength of concrete. Manipulating the microstructure of C-S-H can lead to new cementitious materials with improved structural performance. This paper presents an experimental investigation aiming to characterize a new synthetic polymer-modified synthetic calcium-silicate-hydrate (C-S-H)/styrene-butadiene rubber (SBR) binder. The new C-S-H/SBR binder is produced by calcining calcium carbonate and mixing this with fumed silica (SiO_2), deionized water and SBR. Mechanical, physical, chemical and microstructural characterization was conducted to measure the properties of new hardened C-S-H binder. Results from the experimental investigation demonstrate the ability to engineer a new C-S-H binder with low elastic modulus and improved toughness and bond strength by controlling the SBR content and method of C-S-H synthesis. The new binder suggests the possible development of a new family of low-modulus silica-polymer binders that might fit many engineering applications such as cementing oil and gas wells.

Keywords: Calcium Silicate Hydrate (C-S-H); Polymers; Wellbore Integrity; Binder.

1. Introduction

Portland cement concrete is the most common material used in the construction industry because of its high compressive strength, low cost, constituents' availability, fair durability, and ease in manufacturing. In a micro-scale, concrete possesses a complex structure of multiple calcium silicate phases, which are produced during the cement hydration process [1]. Among those phases, calcium silicate hydrates (C-S-H) represents 60%-70% of the hydrated cement paste and is known to govern the mechanical behavior of concrete at the micro/macro scales. C-S-H also contributed to concrete performance limitations represented by brittleness, low tensile strength, high shrinkage, and microcracking [2,3]. On the other hand, polymers are characterized by their exceptional ductility, flexibility, and durability and therefore have been introduced in composites in various industrial and construction applications [4,5]. To adopt polymers' benefits in concrete, polymer-modified concrete was introduced in the last century with a set of distinct properties, including low permeability, good bond strength, and excellent durability. Polymer-modified concrete was used in various construction applications, specifically in aggressive environments [6,7]. Recent research efforts have been focused on manipulating the microstructure of C-S-H in cement by examining the effect of various pozzolanic additives [8] or by incorporating polymer layers between synthetic C-S-H sheets [9].

Many investigators have conducted extensive studies to characterize C-S-H and have synthesized C-S-H with various procedures and conditions. Beaudoin and Feldman [10] produced synthetic C-S-H by mixing aqueous solutions of calcium oxide (CaO) and sodium metasilicate at various CaO/SiO2 (C/S) ratios while drying of the samples was accomplished by bathing the specimens in acetone and ether. The dried C-S-H powder was then compacted into small discs with compacting pressures ranging from 510-1360 MPa. Alizadeh et al. [11] synthesized C-S-H at C/S ratios between 0.7 and 1.5 to chemically and mechanically simulate C-S-H products found in cement paste. Foley et al. (2012) [12] and Kim et al. (2013) [13], synthesized C-S-H at various C/S ratios using calcium oxide, fumed silica, and deionized water employing different drying techniques to characterize the nanoscale mechanical properties through nanoindentation and thermogravimetric analysis (TGA). Aboubakr et al. (2015) [14], used similar synthesis techniques to establish correlation between the microstructural and viscoelastic properties of C-S-H.

Mechanical properties of synthetic C-S-H were studied by previous researchers [12, 13, 14] reporting elastic modulus and creep compliance of C-S-H via deconvolution analysis of nanoindentation and using dynamic mechanical analysis (DMA) testing. Previous studies show a high discrepancy in elastic modulus of synthetic C-S-H ranging from 3 to 25 GPa varying with the level of compaction pressure ranging from 95 MPa to 500 MPa and the method of testing. The mean elastic modulus of C-S-H compacted at 500 MPa and measured using DMA was reported to be 2.45 GPa [14].

Chemical characteristics of synthetic C-S-H have been identified by numerous research and the formation of an absorbed interlayer of water plays a critical role in the dynamic mechanical properties of C-S-H as described by Alizada et al. (2011) [11]. Silicates make up approximately 75% of hydrated Portland cement paste [3], and manipulation of the microstructural phases and nano-structure of C-S-H is crucial for controlling the properties of concrete on a macro-scale.

Studies have demonstrated that the addition of styrene-butadiene rubber (SBR) creates a polymer network within setting cement that significantly reduces the ultimate compressive strength while increasing the strain at failure [15-18]. Ohama (1995), showed the typical composition of industrial SBR latex which is nearly 50% water by weight with small amounts of surfactant and a vinyl carboxylic acid present [16]. Previous researchers revealed that the addition of polymers to cement creates a film and fills voids within the microstructure [16,17]. This creates an unfavorable interaction between water absorption and polymer hardening of the hydrated and un-hydrated cement particles. The addition of SBR latex to cement based concrete inhibits and strengthens certain mechanical and chemical properties which makes way for the concept of optimizing targeted properties for wellbore applications. SBR latex has shown to have an adverse effect on the formation of C-S-H and Portlandite. The addition of SBR can hinder the hydration process which limits the formation of key components of hydrated cement [18].

While modulus of elasticity values acquired through nanoindentation investigates the microstructural behavior of the material, this work aims to investigate the mechanical properties of C-S-H composites on a larger scale with flexural testing of C-S-H beams. We hypothesize that a new binder of polymer-modified C-S-H can be synthesized with desired properties to fit specific engineering applications such as wellbore applications. The new binder can be engineered to achieve a set of desired characteristics that are not attainable using current cement technology. Such characteristics include low elastic modulus, high bond strength, high strain at failure and low shrinkage. The new binder will significantly reduce the chance of microcracking, due to shrinkage and operation stresses, at the cement-steel and cement-rock formation interfaces improving overall wellbore integrity. We believe that the formation of silicate chains and portlandite in the presence of polymers can be controlled to alter the mechanical and chemical properties of C-S-H. The properties of the hardened synthetic C-S-H/SBR composites are characterized in this paper.

2. Experimental Methods

2.1. Synthesis of C-S-H/SBR composite

Calcium oxide (CaO), also known as quicklime, was produced by calcining reagent grade calcium carbonate ($CaCO_3$), from Mallinckrodt Chemicals, at 900°C. The purity of the lime was greater than 99.5% and was confirmed by weight loss in TGA. Fumed silica (SiO_2) from Sigma Aldrich, with a purity of greater than 99.8% was used as the silicate part in the synthetic C-S-H. Prior investigations showed that the mechanical properties of C-S-H are dependent on CaO/SiO_2 weight ratio (denoted here as C/S ratio) and that at C/S ratio of 1.5 the mechanical properties of C-S-H is similar to that produced by hydrating commercial cement. Therefore, C/S ratio of 1.5 was used herein. Deionized water was added at a 10:1 water-to-binder ratio and the calcium oxide and silica was added at a C/S ratio of 1.5 to produce low viscosity slurry that can be mixed easily. Various amounts of commercial grade SBR latex, ranging from 0 to 15%, by weight of the CaO plus SiO_2 contents, was added to the slurry before mixing. The slurry was placed in a continuous rotary mixer (Fig. 1: Step 1) for seven days at 26°C to allow the C-S-H reaction to fully transpire. The excess water was then extracted by placing the slurry under a vacuum filtering system for 24 hours (Fig. 1: Step 2). The material was then subjected to a standard drying method until the powder achieved 11% relative humidity (RH). All preparation of the materials during synthesis and prior to testing was performed in a nitrogen environment to prevent CO_2 contamination.

The standard method for drying the material to 11% RH used a saturated lithium chloride solution, which allowed reaching a water content that is comparable to cement paste when evaporative water has been removed. The lithium chloride solution was prepared in accordance with the ASTM Standard E 104-02 [19]. The drying system consisted of a 3-beaker set up in series as seen in Fig. 1: Step 3. The beaker containing the saturated lithium chloride was maintained on a hot plate at a constant 50°C ambient temperature. The beaker containing the vacuumed C-S-H, equilibrated to 11% RH for an average of 1 week or until the change in mass was less than 0.1% per day. The last beaker was directly hooked up to the vacuum source with drierite (calcium sulfate and cobalt chloride) to prevent any excess water from entering the vacuum line. This standard drying method was used for all C-S-H preparations due to the relatively quick drying times. Researchers have used this method of drying to equilibrate C-S-H to 11% previously [20–22].

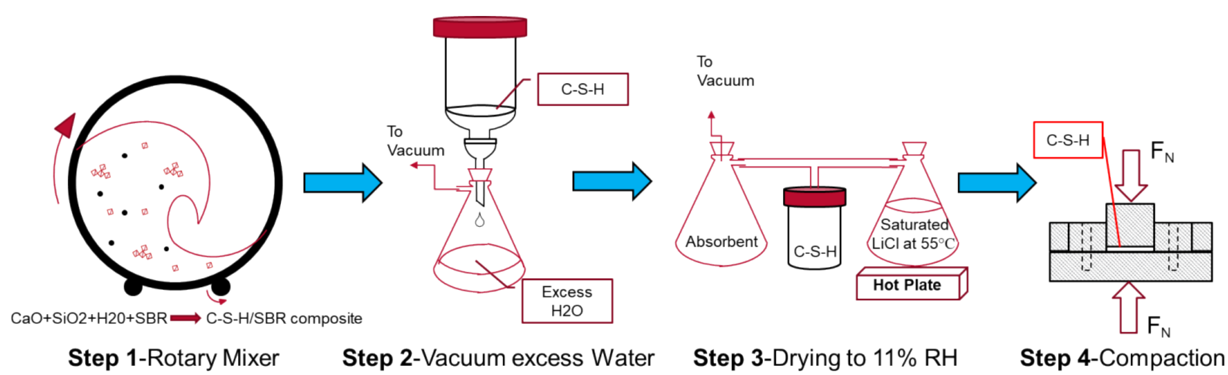

Fig. 1. Synthesis schematic

Compaction was performed by a square, high strength steel mold measuring 200 mm × 200 mm with a small 10 mm × 30 mm insert where the powder to be compacted was placed (Fig. 1: Step 4). The dried C-S-H powder was placed in the insert where the raised inset will apply pressure. Instron Universal Testing Machine was used to induce a compaction pressure of 400 MPa on the

C-S-H powder to achieve levels of porosity and density of 30% and 2000 kg/m^3 , respectively, similar to C-S-H produced by hydrating cement [11,23]. This enables comparing the mechanical properties of the synthetic C-S-H to conventional cementitious binders. A nitrogen environment was not maintained during the compaction, but specimens were immediately moved to the controlled environment once compaction was completed. The compaction loading rate was applied at 1 kN/second and held at the ultimate load for 4 minutes, before unloading completely. A total of 40 specimens 30 mm x 10 mm x 1.8 mm of C-S-H with various amounts of SBR latex were produced using the above procedure prior to conducting mechanical, physical, chemical, and microstructural characterization.

2.2. Mechanical characterization of C–S–H

2.2.1. Dynamic mechanical analysis (DMA)

Dynamic mechanical analysis (DMA) tests were conducted using a TA Instruments, Q800 DMA. DMA was used to characterize the compacted specimens at 25°C and an RH of 11%. The single cantilever setup was used for force-controlled bending testing. The span to thickness aspect ratio of 1:10 was maintained for accurate data acquisition during testing. The test started with an initial static force of 0.002 N and the load was ramped up linearly with a loading rate of 0.5 N/min until failure. Due to the brittle nature of the material, a 0.113 N·m torque was applied with a torque wrench to secure the specimen in the cantilever clamp.

2.2.2. Direct shear test

An ELE International digital shear apparatus was used for the direct shear test. A direct shear test was implemented to examine the bond strength of C-S-H to a steel interface. The compacted C-S-H was carefully removed and placed into the direct shear testing machine (Fig. 2a). After securing the mold into the shearing apparatus and applying the normal force starting at 80 kg, six screws, that held the mold in place during compaction, were removed. A shear force was applied to the top portion of the mold, which contained the confined C-S-H powder as seen in Fig. 2b. A constant displacement rate of 0.90 mm/min was applied while the normal force was held constant for the entirety of the test. Subsequent tests were conducted with the normal force increased in increments of 40 kg ranging from 80 kg to 160 kg. Three replicas for each SBR content were tested.

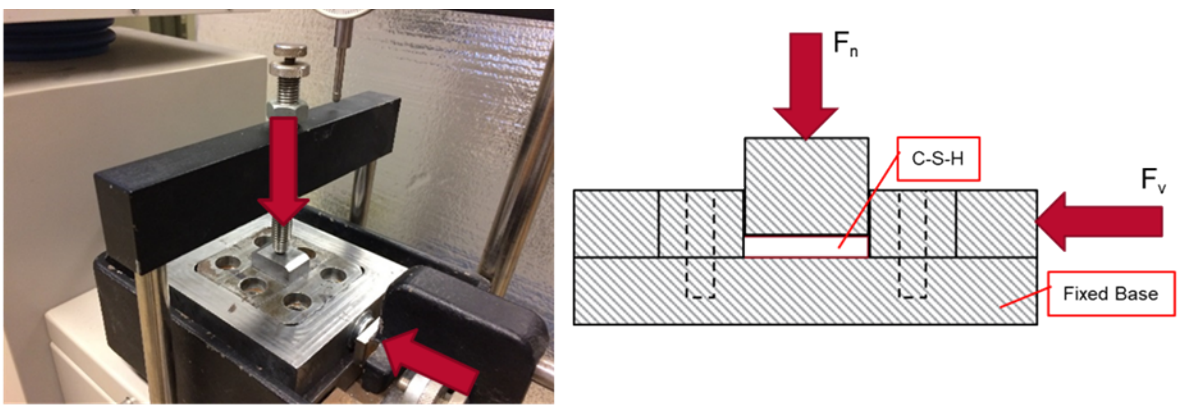

a) Compaction mold in shear apparatus   b) Diagram of shear apparatus

Fig. 2. Direct shear test apparatus and schematic showing load application during test.

2.3. Physical characterization of C-S-H

2.3.1. Density

Density measurements following ASTM C914-95 [24] were used to determine the difference between neat (0% SBR) samples and samples with SBR latex, by calculating the specific modulus and specific strength of the material. Specimens of standard dried C-S-H were compacted at 400 MPa and broken into smaller pieces. The specimens were then weighed using a Mettler Toledo XS-64 and then immediately dipped into paraffin wax until each specimen was entirely coated with wax. The specimens were weighed while submerged in ethyl alcohol. The density was recorded and statistically analyzed.

2.4. Chemical and Microstructural characterization of C-S-H

2.4.1 X-ray diffraction analysis (XRDA)

X-ray diffraction analysis (XRDA) is widely used to detect various chemicals and to investigate the crystalline structures present in a given compound. XRDA was conducted on standard dried C-S-H/SBR specimens and examined to determine how the addition of SBR affects the formation of different microstructural phases of the C-S-H crystalline structure reported by past investigators [12]. C-S-H has a weak crystalline structure due to its amorphous nature and does not produce many strong XRD peaks. The XRD peaks acquired were compared with published results and characterized accordingly. Previous work has shown that CH and C-S-H peaks are shown to dominate the XRD profile for cement pastes. This work also showed a notable phase change with impact on the basal-spacing of C/S mixtures above 1.0 [23,27].

2.4.2. ^{29}Si magic angle spinning (MAS) nuclear magnetic resonance (NMR)

^{29}Si magic angle spinning (MAS) nuclear magnetic resonance (NMR) spectroscopy was performed on standard dried C-S-H powder in 7 mm cylinders spun at 3.6 kHz. An excess of 10,000 scans were performed on each sample resulting in an average testing time of 24 hours. An ASX 300 spectrometer at 59.6 MHz, 7.05 T magnetic field, was used for single pulse analysis without proton decoupling or cross polarization. The ^{29}Si chemical shifts are referenced to $Si(CH_3)_4$ at 0 ppm and with a secondary reference using $Si[(CH_3)_3]_8Si_8O_{20}$ at 11.8 ppm relative to $Si(CH_3)_4$. Hydrated cement exhibits commonly observed chains of Q^1, Q_b^2 and Q^2 typically seen at -79.5, 84.6 and -85.3 ppm respectively. ^{29}Si MAS NMR spectroscopy can determine the polymerization of silicates and describes the mean length *(L)* of silicate chains calculated by the Q^2/Q^1 ratio (Eq. (1)) [21]. The average degree of silicate connectivity, n_c, uses the calculated fractions of Q^n to represent the polymerization of C-S-H (Eq. (2)) [28]. A high n_c value indicates a high degree of polymerization of C-S-H.

$$L = 2(1 + \frac{Q^2}{Q^1}) \tag{1}$$

$$n_c = \frac{Q^1 + 2Q^2 + 3Q^3}{Q^1 + Q^2 + Q^3} \tag{2}$$

2.4.3. Scanning electron microscope imaging (SEM)

Scanning electron microscope (SEM) imaging was conducted on the fractured surface of C-S-H specimens tested by the DMA instrument. The Vega3 Tescan SEM was used to characterize the microstructure of the fractured surface. A secondary electron transmission was used to inspect the surface topography with minimal interference. The specimens were coated with 3-5 nm of carbon as an insulator to enhance the resolution of the microcracks. An accelerating voltage of 15 kV was also used in an effort to optimize the resolution. Careful attention was focused on the microcracks formed on the fractured surface during fracture of the specimens under flexural stresses.

3. Results and Discussion

The flexural stress versus strain curve for C-S-H with various SBR contents is shown in Fig. 3, and the flexural strength is displayed in Fig. 4. The standard C-S-H compacted to 400 MPa without SBR had a modulus of elasticity of 6.6 GPa ± 0.4 GPa. Aboubakr et al. (2015) [14] reported an elastic modulus of 2.45 GPa obtained using DMA testing of C-S-H. Although the rate of loading, sample size, fractions of microstructural phases was different, a comparison between the two studies shows the average elastic moduli of C-S-H is within the same order of magnitude. It is important to note that the elastic modulus obtained using macroscale testing such as DMA is lower than that obtained using nanoscale testing, as reported from nanoindentation tests [13,14]. This is mainly attributed to two facts. First, nanoindentation characterizes individual microstructural phases of C-S-H, while DMA observations represent average modulus of elasticity for all phases due to the difference in the testing scale. Second, as testing scale increases from nano to macro, material porosity and defects increase, leading to reduced properties. It is also worth noting that similar values of modulus of elasticity have been stated for type G oil well cement cured in simulated wellbore conditions [29].

With the addition of SBR, the modulus of elasticity reduces, stress at failure and strain at failure increase along with the toughness (a material's ability to absorb energy to failure). These results demonstrate a common trend as the SBR content increases. For example, the elastic modulus of C-S-H incorporating 15% SBR was reduced by nearly 66% to 2.3 ± 0.3 GPa, as shown in Fig. 4. The specimens also experienced a slightly higher ultimate strength compared with neat C-S-H as the SBR content increases. With the addition of 15% SBR, the flexural strength was 12.3 MPa compared with a flexural strength of 9.7 MPa for neat C-S-H. Specimens of C-S-H with higher contents of SBR displayed early nonlinearity behavior as toughness also increased by approximately 330%, as the content of SBR rose to 15%. T-tests comparing neat C-S-H and C-S-H incorporating 15% SBR produced statistically significant difference when comparing E, ultimate strength, strain at failure, and toughness to samples without SBR. No statistical difference was observed between C-S-H specimens incorporating 10 and 15% SBR. Significantly reducing the E and increasing the strain at failure by 190% and 180% respectively, will limit the propagation of microannulus cracks, thereby limiting potential leakage pathways under wellbore operating conditions.

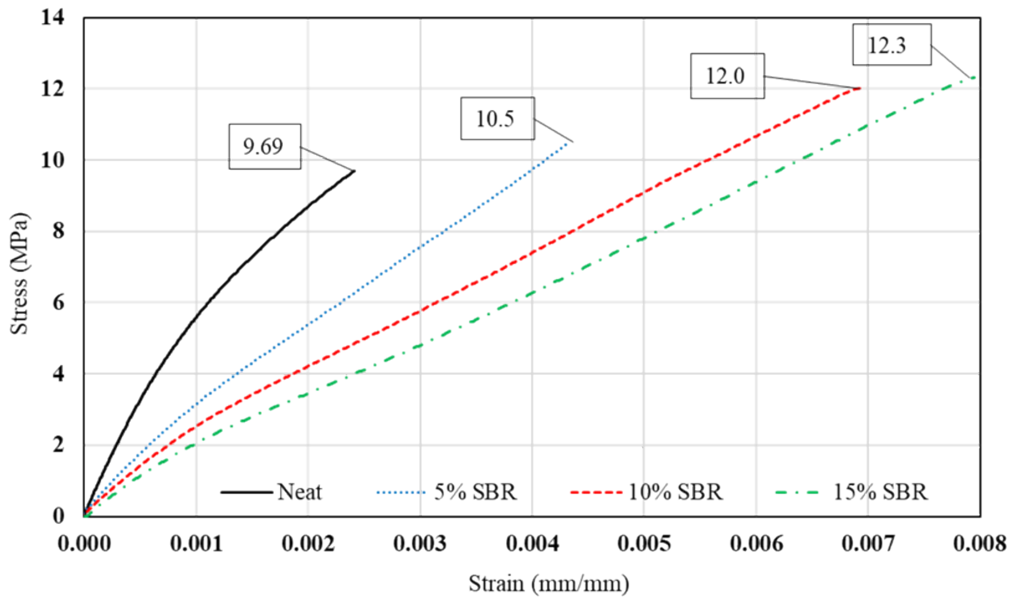

Fig. 3. Stress versus strain curves of C-S-H incorporating SBR obtained using DMA. Boxed numbers represent flexural strength.

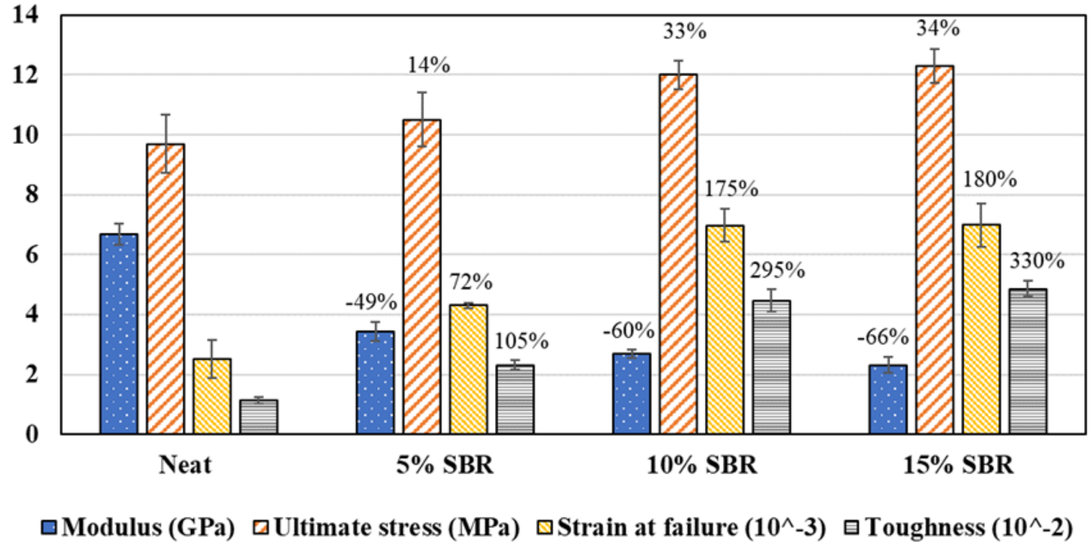

Fig. 4. Mechanical properties of C-S-H/SBR composite obtained using DMA. % above the bars represent the change when compared with neat C-S-H characteristics.

Direct shear tests showed that the bond strength of C-S-H incorporating 15% SBR, to a smooth steel interface, increased by 221% when compared with neat C-S-H. This result also shows a common trend with the incremental increase of SBR. Fig. 5 shows the progressive increase of the bond strength of C-S-H with steel as the SBR content increases. This demonstrates the significant effect of adding SBR for improving bond of synthetic C-S-H to various interfaces. Since the direct shear test is carried out on a C-S-H specimen compacted on the steel surface, it is expected that the measured bond between the C-S-H and steel is mainly frictional. Such a frictional bond is developed due to the slip resistance between the C-S-H and steel surfaces under applied normal stress. Greater improvement in bond strength than observed herein would be expected if the new C-S-H/SBR composite was cast on the steel substrate as an adhesion bond due to a chemical bond between the two surfaces that would have developed in addition to friction bond. A good bond between the new binder and steel could benefit many applications such as cementing oil and gas wells.

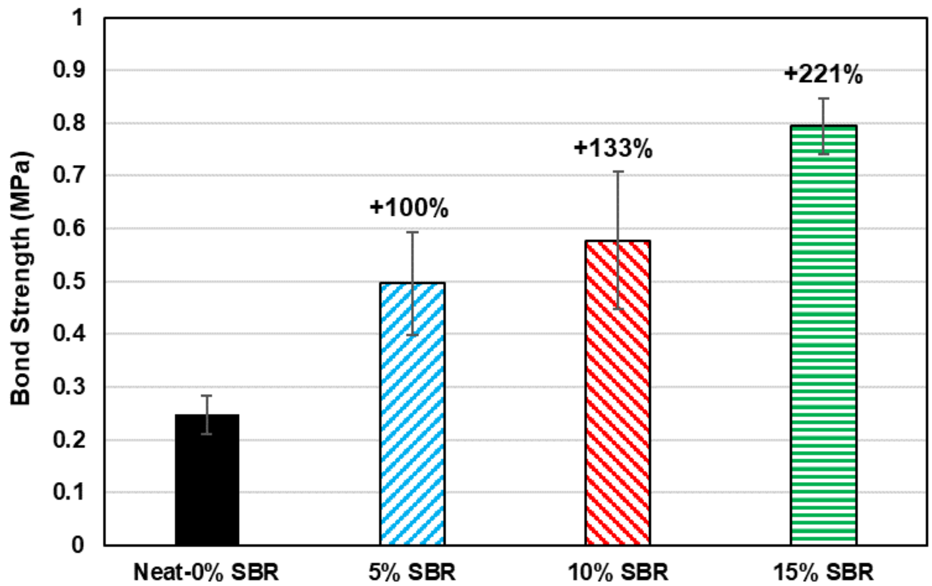

Fig. 5. Bond strength between new binder and steel. % above the bars represent improvement of bond strength when compared with neat C-S-H.

Fig. 6 shows a slight decrease in density of C-S-H with the incorporation of SBR. The density of neat C-S-H is in the same range reported by other researchers [11,12]. Material property charts allow C-S-H to be categorized and compared with other materials in the material performance chart. Material property charts for C-S-H with various SBR contents are established using elastic modulus and density as shown in Fig. 7. Fig. 7 also shows the C-S-H neat samples located in a different region than a cluster of C-S-H incorporating. The neat C-S-H falls in the nontechnical ceramic classification which includes concrete, ceramics, and clay bricks. The samples incorporating SBR fall in between the concrete and polymers material classification [30]. This is indicative of a material performance deviation and directly correlates to the low modulus and high ultimate strength of C-S-H incorporating SBR. These observations demonstrate the ability to engineer new species of polymer-silica binders with physical and mechanical characteristics that is desired for wellbore applications and might be of interest to other engineering applications.

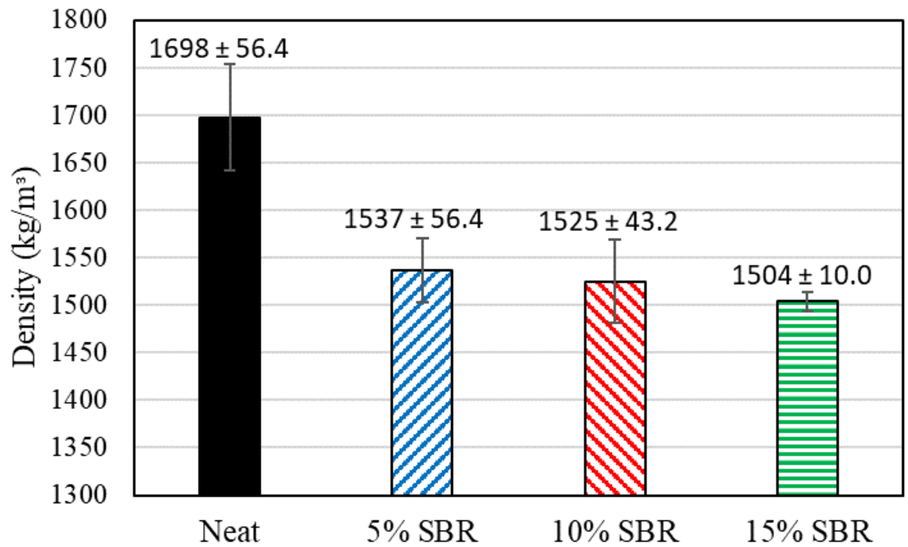

Fig. 6. Density measurements of C-S-H with standard deviation

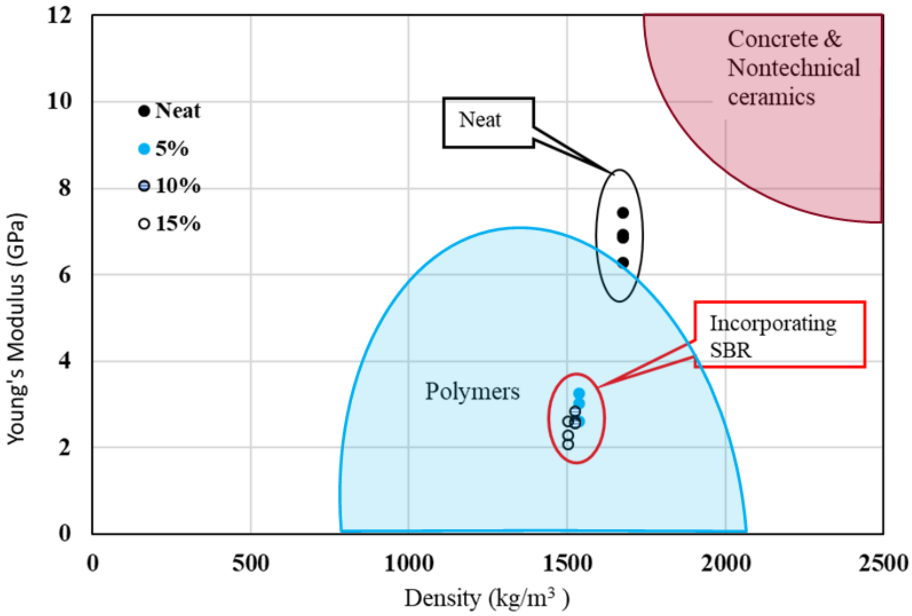

Fig. 7. Material performance indices for C-S-H/ SBR composite with various SBR contents compared with neat C-S-H.

XRD measurements as demonstrated in Fig. 8 showed typical peaks representing C-S-H phases along with CH. Outcomes were confirmed by comparison with published results [13]. The formation of the crystalline structure of C-S-H has negligible change as the SBR content increases. Peaks at 29°, 32°, and 48° represent the formation of C-S-H and coincide with previous investigations [13,25]. The presence of CH is represented by slim spikes at 18° and 34°. Due to the peaks for $CaCO_3$ occurring at 29.5°, XRDA typically does not pick up indications of $CaCO_3$. Other signals of $CaCO_3$ are lost in background noise. Peaks obtained from the XRD spectra for C/S=1.5 matched well with published results [13].

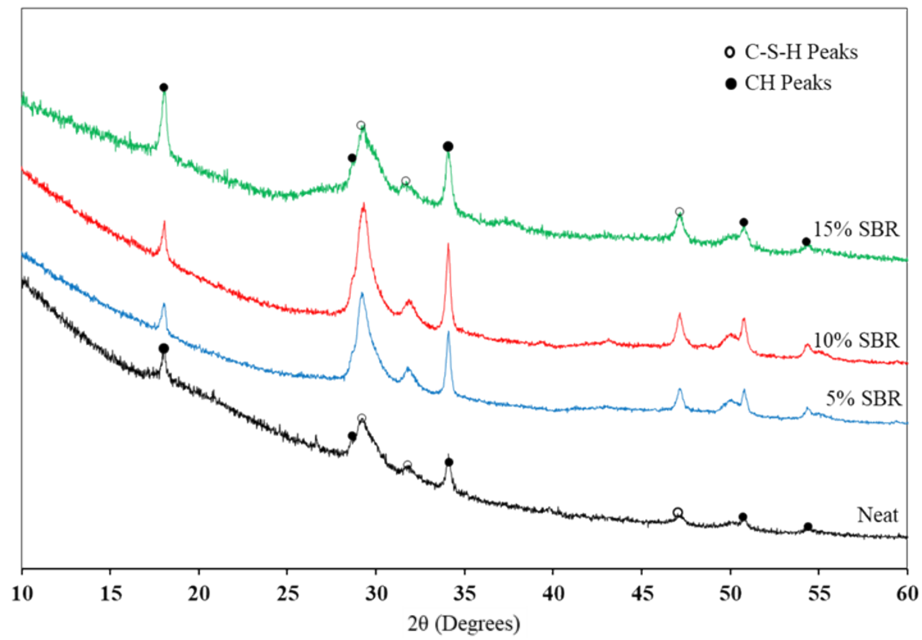

Fig. 8. XRDA spectrum of neat C-S-H and C-S-H incorporating varying amounts of SBR. Slim peaks at 18° and 34° represent CH and the peaks at 29° and 32° represent C-S-H.

NMR spectra of C-S-H neat and with varying amounts of SBR depicted in Fig. 9. The vertical lines at -78.9, -82.6, and -85 ppm represent crystalline connectivity at correlating to Q^1, Q^2_b, and Q^2 silicate connections respectively [13]. Deconvolution analysis was performed to determine the approximate fractions of each crystalline phase and can also be seen in Fig. 10.

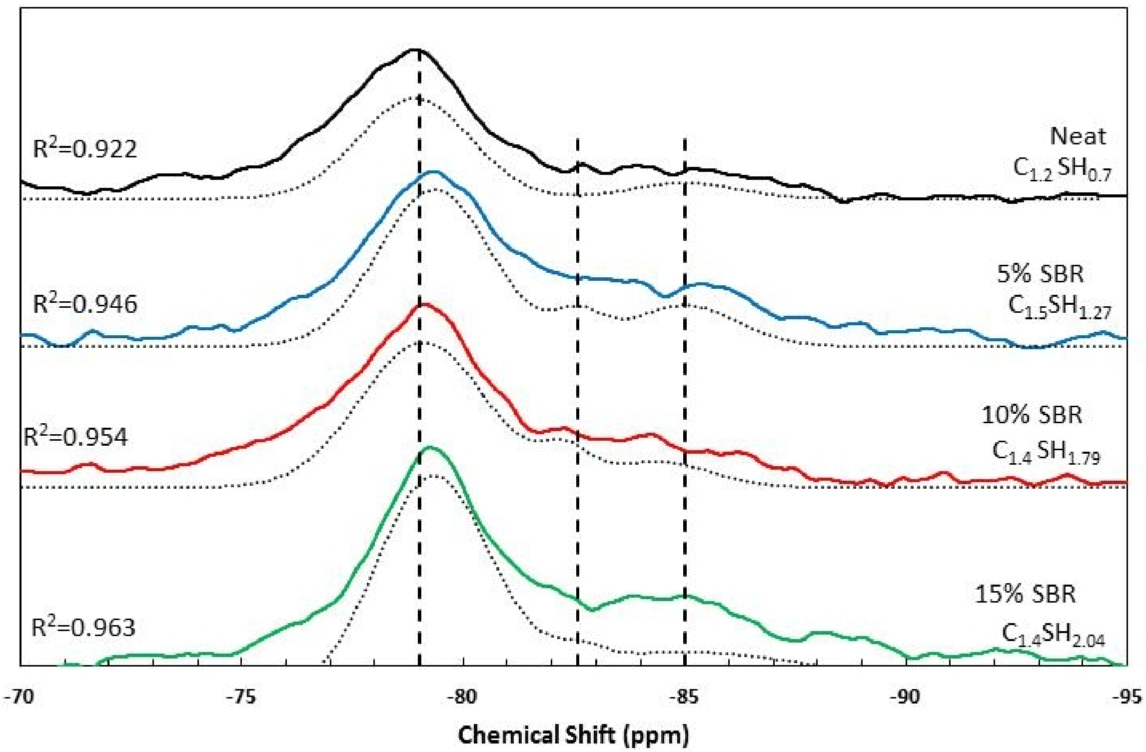

Fig. 9. ^{29}Si solid-state NMR Spectra with deconvolution curves (dotted line)

The negative chemical shifts at Q^1 and Q^2 sites, associated with the SBR content increases, may indicate an increase in the degree of silicate tetrahedra polymerization [24]. The results of the deconvolution analysis of ^{29}Si MAS NMR spectra are presented in Table 1. Values of silicate end chains, represented by Q^1, also increased along with Q^2_b signals as SBR content increased. This is thought to happen as the interlayer of water assists in forming new Q^2 and Q^2_b chains. Q^2_b represents a single bridging site creating a middle tetrahedron in the C-S-H chain that links the Q^2 species and chain-end Q^1 [31]. As the inner layer of water becomes trapped, due to the polymer film, the dissipation of the inner water layer creates shielding and crosslinking mechanisms between the C-S-H layers, resulting in more Q^2 formations [24]. Mean chain lengths (L) remained constant at 2.81±0.07 while values of n_c, representing a high degree of C-S-H polymerization, decreased from 1.97 to 1.28 with the increase of SBR content and coincides with published results [13].

Table 1. Q^n intensities extracted from the deconvolution of ^{29}Si MAS NMR spectra.

C-S-H Formula	SBR %	Q^1	Q^2_b	Q^2	Q^2/Q^1	n_c	L
$C_{1.2}SH_{0.7}$	0%	0.695	--	0.305	0.439	1.97	2.88
$C_{1.5}SH_{1.27}$	5%	0.706	0.178	0.115	0.163	1.29	2.83
$C_{1.4}SH_{1.79}$	10%	0.714	0.178	0.107	0.150	1.29	2.80
$C_{1.4}SH_{2.04}$	15%	0.730	0.090	0.180	0.246	1.27	2.74

To further explain the improvement in mechanical properties, SEM images of the fractured surface was investigated. SEM images for neat C-S-H and C-S-H incorporating 15% SBR are shown in Fig. 10. SEM imagery provided some visual insight for the physical effects of SBR on the fracture characteristics of C-S-H incorporating SBR. Microcracks were observed on the fracture surface of the specimens after DMA testing. When comparing the fractured surface of neat C-S-H with C-S-H incorporating 15% SBR (Fig. 10b-10c), it is noted that SBR films are bridging the microcracks, leading to improvements in ductility and strength. Fig. 10c provides a close-up of a micro-fracture, giving a perspective on how effective SBR is at limiting the propagation of the micro-cracks enabling the composite C-S-H-SBR to continue carrying loads and provide a relatively high strain at failure.

Finally, a hypothesis to explain the chemical and mechanical behavior of C-S-H incorporating SBR is depicted in Fig. 11. The proposed hypothesis is adapted from the modern colloidal/gel-like microstructure model of C–S–H by Dolado et al. [32] and the nanostructure of polymer-modified C-S-H structure suggested by Raki et al. [33]. The figure compares the microscale structures of neat C-S-H in Fig. 11(a) and C-S-H with SBR latex in Fig. 11(b). In neat C-S-H, voids and micro-cracks exist between the calcium silicate sheets due to shrinkage and applied stresses. On the other hand, incorporating SBR latex in C-S-H production yields a network of SBR film capable of bridging between calcium silicate sheets, as observed in SEM investigation (Fig. 10). At the nanoscale, SBR polymer chains are built within the calcium silicate sheets, as demonstrated in Fig. 11 (c). The nano and microstructure changes of C-S-H modified with SBR lead to novel polymer-modified tobermorite-like structure with improved mechanical properties (i.e., strength, stiffness, and strain capacity). The multiscale interaction mechanisms of polymers in C-S-H were suggested earlier by Raki et al. [33].

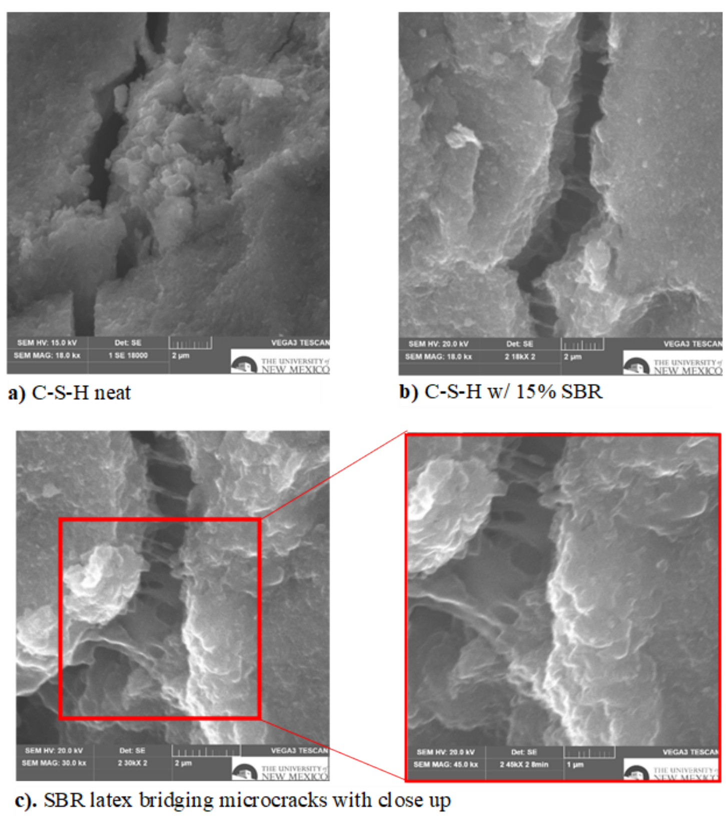

Fig. 10. (a)–(c) SEM micrographs of fractured surface of C-S-H incorporating SBR

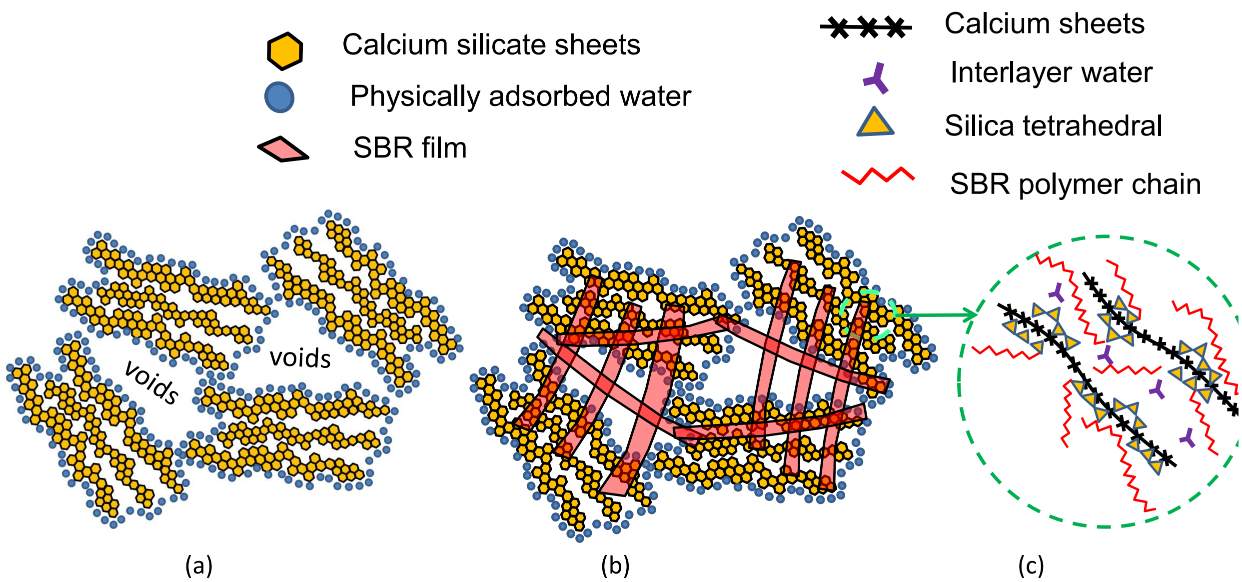

Fig. 11. Schematic representation of physical model of SBR film inhibiting the formation of C-S-H (a) neat C-S-H, (b) SBR film network bridging C-S-H sheets, and (c) SBR polymer chains build on silicate crystalline structure

It is suggested herein that the OH groups in the SBR might react with the Ca and Si in the C-S-H, leading to the formation of Ca-OH and Si-OH bonds that is not typically observed in neat C-S-H. Raki et al. [33] indicated several mechanisms of interaction between polymers and C-S-H. Among those mechanisms, the alkyl chains in a polymer can covalently bond to silica sheets to form a bilayer between the sheets. Further research is warranted using analytical chemistry methods (e.g., Fourier Transform Infrared - FTIR) to prove this reaction.

The above research is a purely fundamental work that represents initial steps towards producing polymer-modified silica-based binders that enables controlling key mechanical properties desired in wellbore applications, specifically low modulus, high strain at failure and high bond strength. The above investigation showed that the new C-S-H/SBR composite has numerous favorable characteristics for wellbore applications including low elastic modulus and thus low stresses during cyclic and thermal operations, improved bond strength, improved tensile strength and significantly improved failure strain and toughness. All the above improvements suggest that the new low modulus C-S-H/SBR binder might be an excellent candidate for wellbore applications. The new binder might also be useful for other engineering applications with similar operational conditions. It is important to note that the limited content of the SBR in the mix will limit the cost of the new binder. Considering the combined weight of CaO and SiO_2 with the recommended use of 10-15% SBR, a 15% increase in cost can be anticipated. In view of the significant reduction of probability of cracking of the new binder compared with current cementing technology, one can show such cost increase to be very marginal.

The proposed binder would not be possible by adding SBR to cement during cement hydration, in what is known today as polymer-modified cement, but by incorporating SBR into the cement particles during cement manufacturing. Challenges associated with the binder manufacturing is thus related to methods to incorporate polymer components into the cement manufacturing process. Further research is warranted to examine methods to fabricate the new binder. It is not the scope of this work to suggest the method to produce the new binder. It is the authors' interest to show that when such a binder is made, its C-S-H will entertain low modulus, high strain at failure and improved bond strength, which are desirable mechanical properties for wellbore and other engineering applications.

4. Conclusions

C-S-H was synthesized from a CaO/SiO_2 ratio of 1.5 to mimic C-S-H formed in oil well cement applications. The synthetic C-S-H was dried to 11% RH, compacted to 400 MPa and characterized by various methods. Mechanical properties acquired from DMA and direct shear testing, along with chemical properties from TGA and microstructural characteristics with XRDA, ^{29}Si MAS NMR and SEM were acquired to characterize the effect due to incorporating SBR latex. DMA results showed the ability to control Young's modulus of elasticity while increasing the ultimate tensile strength capacity and toughness of C-S-H. The material performance indices of specimens containing SBR showed a clear deviation from the neat specimens. Neat C-S-H lies in the concrete classification and the C-S-H/SBR composite lies between the concrete and polymer regions on the material classification index. TGA curves revealed the formation of the C-S-H structure with increased inner water layers due to the addition of SBR. XRDA did not display any adverse effect on the C-S-H formation due to the addition of SBR. NMR spectra displayed a negative shift for C-S-H with SBR indicating a higher degree of silicate polymerization. Furthermore, SEM imagery shows SBR particles spanning the microcracks on the fracture surface, providing insight on the enhanced mechanical properties of the new C-S-H/SBR binder. The above work demonstrates the ability to engineer a new low-modulus binder for various engineering applications with improved mechanical properties with the addition of various amounts SBR during C-S-H synthesis. The new binder has a lower probability of cracking and debonding from the steel than current cements used in wellbore applications.

Acknowledgments

The authors would also like to thank Dr. Hien, Dr. Eric Peterson, Mike Spidle and Dr. Karen Ann Smith from UNM and Dr. Usama Kandil from EPRI (Egypt) with their help in conducting the microstructural analysis. This research was funded by Sandia National Laboratories LDRD program, project 200181. The authors greatly acknowledge this support. We thank David Sassani for providing a technical review of this work.

Sandia National Laboratories is a multimission laboratory managed and operated by National Technology and Engineering Solutions of Sandia, LLC, a wholly owned subsidiary of Honeywell International, Inc., for the U.S. Department of Energy's National Nuclear Security Administration under contract DE-NA-0003525. SAND2019-xxxx. This paper describes objective technical results and analysis. Any subjective views or opinions that might be

expressed in the paper do not necessarily represent the views of the U.S. Department of Energy or the United States Government.

References

[1] M. Schneider, M. Romer, M. Tschudin, H. Bolio, Sustainable cement production—present and future. Cement Concr. Res., 41(2011), 642-650.

[2] C. Alonso, L. Fernandez, Dehydration and rehydration processes of cement paste exposed to high temperature environments. J. Mater. Sci., 39(2004), 3015-3024.

[3] P.J.M. Mehta, P. K., Monteiro, Concrete Microstructure, Properties, and Materials, 4th ed., McGraw Hill, USA, 2013.

[4] K. Balani, V. Verma, A. Agarwal, R. Narayan, Physical, thermal, and mechanical properties of polymers. Biosurfaces: A Materials Science and Engineering Perspective, (2015), 329-344.

[5] W. R. Ashcroft Industrial polymer applications: essential chemistry and technology. Royal Society of Chemistry, (2019).

[6] J. B. Kardon, Polymer-modified concrete. J. Mater. Civ. Eng, 9(1997), 85-92.

[7] B. Liu, J. Shi, M. Sun, Z. He, H. Xu, J. Tan, Mechanical and permeability properties of polymer-modified concrete using hydrophobic agent. J. Build. Eng., (2020), 101337.

[8] L. Wang, F. Guo, Y. Lin, H. Yang, S. W. Tang, Comparison between the effects of phosphorous slag and fly ash on the CSH structure, long-term hydration heat and volume deformation of cement-based materials. Constr. Build. Mater., 250 (2020), 118807.

[9] M. Kamali, A. Ghahremaninezhad, A study of calcium-silicate-hydrate/polymer nanocomposites fabricated using the layer-by-layer method. Mater., 11(2018), 527.

[10] J. J. Beaudoin, R. F., Feldman, Dependence of degree of silica polymerization and intrinsic mechanical properties of C-S-H- on C / S ratio, Int. Congr. Chem. Cem. 6 (1986) 1–6.

[11] R. Alizadeh, J.J. Beaudoin, L. Raki, Mechanical properties of calcium silicate hydrates, Mater. Struct. Constr. 44 (2011) 13–28. doi:10.1617/s11527-010-9605-9.

[12] E.M. Foley, J.J. Kim, M.M. Reda Taha, Synthesis and nano-mechanical characterization of calcium-silicate-hydrate (C-S-H) made with 1.5 CaO/SiO2mixture, Cem. Concr. Res. 42 (2012) 1225–1232. doi:10.1016/j.cemconres.2012.05.014.

[13] J.J. Kim, E.M. Foley, M.M. Reda Taha, Nano-mechanical characterization of synthetic calcium-silicate-hydrate (C-S-H) with varying CaO/SiO2mixture ratios, Cem. Concr. Compos. 36 (2013) 65–70. doi:10.1016/j.cemconcomp.2012.10.001.

[14] S.H. Aboubakr, M.L. Begaye, U.F. Kandil, M.R. Taha, Multi-scale Viscoelastic Characterization of Synthetic C-S-H, 5th Int. Symp. Nanotechnol. Constr. (2015).

[15] N. Shirshova, A. Menner, G.P. Funkhouser, A. Bismarck, Polymerised high internal phase emulsion cement hybrids: Macroporous polymer scaffolds for setting cements, Cem. Concr. Res. 41 (2011) 443–450. doi:10.1016/j.cemconres.2011.01.017.

[16] Y. Ohama, Handbook of polymer-modified concrete and mortars: properties and process technology, William Andrew, 1995.

[17] D. Van Gemert, A. Beeldens, Evolution in modeling cement hydration and polymer hardening in polymer-cement concrete, Adv. Mater. Res. 687 (2013) 291–297. doi:10.4028/www.scientific.net/AMR.687.291.

[18] X.B. Yue, R. Wang, Influence of SBR latex on the formation of C-S-H in C3S paste, Adv. Mater. Res. 687 (2013) 329–334. doi:10.4028/www.scientific.net/amr.687.329.

[19] 104-02 ASTM Standard E, Standard Practice for maintaining Constant Relative Humidity by Means of Aqueous Solution., ASTM Int., West Conshohocken, PA, 2007.

[20] V.S. Feldman, R. F., & Ramachandran, Differentiation of interlayer and adsorbed water in hydrated Portland cement by thermal analysis, Cem. Concr. Res. 1 (1971) 607–620.

[21] W. Young, J. F., & Hansen, Volume relationships for CSH formation based on hydration stoichiometries, MRS Online Proc. Libr. Arch. 85 (1986).

[22] A.J. Thomas, J. J., Jennings, H. M., & Allen, The surface area of cement paste as measured by neutron scattering: Evidence for two C-S-H morphologies, Cem. Concr. Res. 28 (1998) 897–905.

[23] R.A. Alizadeh, Nanostructure and Engineering Properties of Basic and Modified Calcium-Silicate-Hydrate Systems, (2009) 250. doi:10.13140/RG.2.1.3892.8089.

[24] 914-95 ASTM Standard C, Standard test method for Bulk Density and Volume of Solid Refractories by Wax Immersion, ASTM Int., PA, 2004: pp. 187–189.

[25] Taylor, H. F. (1997). Cement chemistry (Vol. 2). London: Thomas Telford.

[26] Kaw, A. K. (2005). Mechanics of composite materials. CRC press.

[27] J. Jain, N. Neithalath, Physico-chemical changes in nano-silica and silica fume modified cement pastes in response to leaching, Int. J. Mater. Struct. Integr. 3 (2009) 114–133. doi:10.1504/IJMSI.2009.028608.

[28] G. Le Saout, E. Lécolier, A. Rivereau, H. Zanni, Chemical structure of cement aged at normal and elevated temperatures and pressures, Cem. Concr. Res. 36 (2004) 71–78. doi:10.1016/j.cemconres.2004.09.018.

[29] O. Guner, D., Ozturk, Comparison of Mechanical Behaviour of G Class Cements for different Curing Time, (2015) 445–451.

[30] M. Ashby, Materials selection in mechanical design, 5th Edition, Butterworth-Heinemann, Elsevier, (2017).

[31] Q. Li, A. P. Hurt, N. J. Coleman, The Application of ^{29}Si NMR Spectroscopy to the Analysis of Calcium Silicate-Based Cement Using Biodentine™ as an Example, Journal of Functional Biomaterials, (2019) 10, 25, doi:10.3390/jfb10020025

[32] J. S. Dolado, M. Griebel, J. Hamaekers, F. Heber, The nano-branched structure of cementitious calcium–silicate–hydrate gel. J. Mater. Chem., 21(2011), 4445-4449.

[33] L. Raki, J. Beaudoin, R. Alizadeh, J. Makar, T. Sato, Cement and concrete nanoscience and nanotechnology. Mater., 3(2010), 918-942.